RSC Advances

SCHOLARONE™
Manuscripts

RSC Advances

Fast and facile preparation of PEGylation graphene from graphene oxide by lysosome targeting delivery of photosensitizer to efficiently enhance photodynamic therapy

Yiping Zeng,[a1] Zhangyou Yang,[a1] Shenglin Luo,[a] Hong Li,[a] Cong Liu,[a] Yuhui Hao,[a] Jing Liu,[a] Weidong Wang [b],* and Rong Li [a],*

Graphene with unique physical and chemical properties has shown various potential applications in biomedicine. In this study, a fast, facile and mass production method was reported to obtain stable and disperse polyethylene glycol (PEG) modified nanographene (NGO-PEG, 20~40 nm) by covalently functionalized with a linear chain PEG. X-ray photoelectron spectroscopy and UV/Vis indicated the successful preparation of NGO-PEG. Atomic force microscopy was used to demonstrate the structure and size of GO and NGO-PEG. The branched polyethylenimine (BPEI) modified NGO-PEG (NGO-PEG-BPEI) was strategically designed and prepared as the targeting drug delivery system to achieve higher specificity. The photosensitizer molecule Chlorin e6 (Ce6) was loaded onto NGO-PEG and NGO-PEG-BPEI via π-π stacking and hydrophobic interactions. The obtained NGO-PEG-Ce6 and NGO-PEG-BPEI-Ce6 show excellent photodynamic efficacy compared to free Ce6 because of the significantly enhanced intracellular delivery of Ce6. The NGO-PEG-BPEI-Ce6 offers a remarkably improved photodynamic efficacy. The drug loading capability, cell uptake, intracellular localization and ROS-producing ability were discussed to explain why NGO-PEG-BPEI-Ce6 had higher photodynamic efficacy than free Ce6 and NGO-PEG-Ce6. Our study highlights a green route to synthesize stable and disperse NGO-PEG, and identifies a role for NGO-PEG-BPEI as a carrier to target lysosomes to improve the efficacy of photodynamic therapy.

Introduction

Graphene has emerged as a flat monolayer of carbon atoms that are tightly packed into a two-dimensional (2D) honeycomb lattice. There have been extensive research activities on graphene in recent years because of its unique shape/size as well as various intriguing physical and chemical properties.[1-7] Based on the advantages, graphene and its derivative graphene oxide (GO) have been widely investigated for applications in nanoelectronic device,[8] transparent conductors, nanocomposite materials,[9] energy research and catalysis. Owing to these high optical absorption in the near-infrared (NIR) region, graphene and GO have been extensively applied for photothermal therapy (PTT).[10] In addition, graphene and GO with an extremely high specific surface area can interact with various biomolecules for applications in biosensor, drug delivery, gene transfection and photodynamic therapy (PDT). [11-15]

However, graphene is hydrophobic and readily agglomerates in hydrophilic solvents such as water and physiological solutions.[9] It is well known that nanoparticles without sufficient surface protection inevitably encounter many obstacles in vivo.[16, 17] Therefore, the key challenge in the synthesis and application of bulk-quantity graphene is the prevention of aggregation. Previous reports show that the attachment of other molecules or polymers on the graphene can reduce the aggregation by covalent or noncovalent strategies.[18] Polyethylene glycols (PEG),[13] sulfonic acid groups,[19] chitosan [20] and polyacrylic acid [21] have been previously explored to prevent the aggregation via covalent interactions, and other groups have used Tween [22] or Pluronic F127 [23] as a stabilizer to prevent the aggregation of graphene via noncovalent interactions. PEG functionalization is a major approach to modify nanocarrier, because it can prolong the circulation time of the pharmaceuticals in blood and avoid rapid uptake by macrophages of the mononuclear phagocyte system (MPS). Recently, some studies showed that six-armed PEG was conjugated to GO using the EDC/NHS reaction with significantly improved biocompatibility and water solubility in physiological solutions.[13] However, this method is not simple and efficient because there is insufficient number of carboxylic acid functional groups located at the edge of graphene. Therefore, to introduce abundant carboxylic acid functional groups, GO was exfoliated by free-radical addition,[24] GO must been placed in a strongly alkaline condition[13] (1.5 M NaOH) with bath-sonicating

[a] State Key Laboratory of Trauma Burns and Combined Injury, Institute of Combined Injury, Chongqing Engineering Research Center for Nanomedicine, College of Preventive Medicine, Third Military Medical University, Chongqing 40038, China

[b] Department of Radiation Oncology, Shanghai Sixth People Hospital, Shanghai Jiao Tong University, Shanghai 200233, China.

* Address correspondence to lrong361@126.com and wwdwyl@sina.com

† Electronic Supplementary Information (ESI) available: See DOI: 10.1039/x0xx00000x

and heat treating (55℃).[25] However, another study showed a different opinion that exfoliated GO can experience fast deoxygenation in strongly alkaline solutions (0.1 M NaOH) at moderate temperatures (50–90℃),[26] then stable aqueous graphene suspensions were obtained without carboxylic acid functional groups on the GO plane. Thorough investigation is required to understand the exact opinion of carboxylated GO. In addition, the PEG chain reacts with the carboxylic acid functional groups located at the edge of graphene which severely restricts its promising application. Furthermore, EDC/NHS chemistry couldn't perform large-scale productivity. Hence, the aforementioned limitations inspired us to explore a simple, facile and high-efficiency method for preparation of PEGylation nanographene (NGO-PEG).

PDT is known as an increasingly recognized alternative to treat various cancers in clinical practice.[27, 28] Under the irradiation of light with an appropriate wavelength, the photosensitizer (PSs) molecule transfers the photon energy to the surrounding oxygen molecules to generate reactive oxygen species (ROS) , such as singlet oxygen, to kill cancer cells.[29-31] Compared with chemotherapy or radiotherapy, PDT shows relatively reduced side effects and improved tumour-specific killing. Meanwhile, the subcellular localization of PSs dictates the primary site of damage and the consequent outcome of the treatment, implying direct cell damage and secondary effects.[32] The photosensitizers preferentially accumulate in specific organelles (e.g. late endosomes/lysosomes, mitochondria, or the endoplasmic reticulum),[33] then, the efficiency of PDT is significantly improved due to the specific organelle photodamage after irradiation. In particular, the ER and/or mitochondria photodamage triggers a pro-survival autophagic response to recycle injured organelles. Conversely, the efficacy of lysosomal photodamage may be partly from both promotion of autophagic stress and suppression of autophagic prosurvival functions. It appears that lysosomes may be the optimal target to improve the efficacy of PDT. However, the hydrophobic nature of most PSs results in strong self-aggregation in aqueous media, which significantly reduces their photodynamic efficacy because only monomeric species are appreciably photoactive.[34] Hence, in order to increase the water solubility of PSs molecules and improve their delivery into cancer cells, various nanocarriers have been actively developed for the delivery of PDT agents,[35] such as nanographene, polymer nanoparticles, gold nanoparticles, magnetic nanoparticles, silica nanoparticles, and so on.[36-38]

In our strategy, a unique NGO-PEG design was developed for intracellular PSs delivery. The findings enable GO materials processing with low-cost, facile processing techniques and mass production. GO has been suggested to contain plentiful reactive epoxy groups on either side of its basal plane.[39] Therefore, a nucleophilic ring-opening reaction should easily occur between the epoxy groups of GO and the amine-functional molecules with the catalysis of potassium hydroxide (KOH). In this work, the resulting introduction of the hydrophilic amine-terminated PEG to the graphene plane should result in a well dispersible graphene-based material. Significantly, the carboxylic acid functional groups located at the edge of graphene are retained for further functionalization. Thus, via covalent interaction, polyethyleneimine (PEI)[40] or FA[41] molecules should react with the carboxylic acid functional groups of GO for further biological application. Herein, polyethylenimine-modified NGO-PEG (NGO-PEG-PEI) was also prepared as a drug delivery system. Otherwise, compared to the negatively charged carboxylated of NGO-PEG, the positively charged NGO-PEG-PEI may be more uptaken by cancer cells lines,[42] so the latter was able to

enhance the intracellular delivery of PSs for improved PDT efficiency. In this work, we show that NGO-PEG-PEI not only has a high PDT agents (Chlorin e6, Ce6) loading capability but also shows excellently lysosomes target property compared to NGO-PEG which located in the cytoplasm. Meanwhile, the PDT efficiency of NGO-PEG-PEI-Ce6 was much higher than that of NGO-PEG-Ce6 and free Ce6. The cell uptake and ROS producing ability of the functionalized graphene-based material were evaluated carefully for future explores *in vivo* applications of these biomaterials.

Results and discussion

Scheme 1 illustrates the synthetic pathway for making the NGO-PEG-Ce6 and NGO-PEG-BPEI-Ce6. Firstly, GO was prepared by oxidizing graphite according to a modified Hummer's method.[43] X-ray diffraction analysis was carried out to confirm the product. The result shows that the GO was synthesized successfully (Fig. S1). NGO was obtained by ultrasonic probe cracked GO. The size and morphology of the GO and NGO-PEG were characterized by atomic force microscopy (AFM) (Fig. 1). As showed in Fig. 1a, the size and thickness of the unmodified GO were about 100~500 nm and ~1.0 nm respectively which suggest a single-layer graphene sheet and consistent with previous reports. Catalyzed by potassium hydroxide (KOH), the ring-opening reaction was occurred between the epoxy groups of NGO and the amine groups of PEG-amine under at moderate temperatures (80℃). With the reaction ongoing, the colour of aqueous solution changed from yellowish-brown to dark-black (Fig. 1c&d inset). Unexpectedly, the size of NGO-PEG was found about 20-40 nm and ~1.4 nm thickness (Fig. 1b). The increased thickness may mainly due to the attachment of PEG on both planes of the NGO sheet. In order to illustrate the covalent functionalization between NGO and PEG, X-ray photoelectron spectroscopy (XPS) was performed on NGO and NGO-PEG samples (Fig. 1c&d). The XPS survey spectrum of NGO-PEG showed a nitrogen peak around 400 eV, whereas no N signal can be observed for the NGO. As shown in the inset of Fig. 1d, the N1s band appeared at 401.9 eV with a lower binding energy shoulder at 399.8 eV,[44] confirming the presence of NH units in modified NGO-PEG sheets. The XPS result indicates that the covalent reaction between amino group of PEG and the epoxy group on GO sheets occurred successfully.

In this study, detailed conditions experiments were investigated to evaluate the effects on NGO-PEG prepared, including (a) considering the influence of raw material , only presence amine-PEG-5000 or KOH (Fig. 2a). (b) different functional
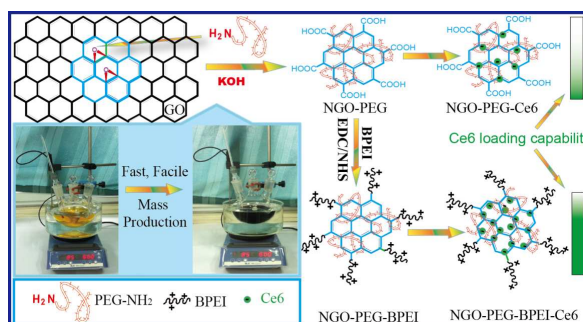
Scheme 1 Synthetic procedure of NGO-PEG-Ce6 and NGO-PEG-BPEI-Ce6

group (Fig. 2b), (c) small molecules (Fig. 2c), (d) different PEG chain length (Fig. 2d). As shown in Fig. 2e, the dispersible, stabilized and reduced size NGO-PEG was successfully prepared when both PEG and KOH were presence. The conversion yield from NGO to NGO-PEG was nearly 100 % without aggregation. Conversely, in presence of PEG or KOH individually under the identical conditions, precipitate was visibly obtained (Fig. 2e). The results show that PEG and KOH were the equally important for this synthesis reaction. Furthermore, in order to study whether the interaction between PEG and NGO is covalently bonded or noncovalently bonded, three different PEG-based materials (PEG-OH, PEG-COOH and PEG-NH$_2$) were investigated. Among these anchor groups, Fig. 2f shows that PEG-OH and PEG-COOH stabilized NGO were agglomerated and thus visibly precipitated under the same conditions as used in the final synthesis. However, the PEG-NH$_2$ stabilized NGO was stable even after it was centrifuged. In short, only the amino functional group could anchor to the NGO plane to stabilize it, which demonstrates that the interaction between PEG and NGO is not physical absorption but covalently bonded between amino functional group and epoxy bond. Next, small molecules that involve amino groups were also investigated to determine whether the small molecules can stabilize NGO. The result indicated that the four types of small molecules modified NGO were subjected to agglomeration and thus visibly precipitated under the same conditions as used in the final synthesis, and not passes filters with a cutoff of 0.22 μm. Therefore, the NGO could not been stabilized by small molecules even though they had the amino group (Fig. S2a). Then, we analyzed that the chain length was the critical factor for the failure of small molecules stabilized NGO. Herein, amine-PEG-350, amine-PEG-2000 and amine-PEG-5000 were selected to investigate the influence of different chain length. As shown in Fig. S2b that amine-PEG-350 and amine-PEG-2000 functional NGO did not pass filters with a cutoff of 0.22 μm partially, which demonstrated that they instantaneously formed agglomerates larger than 0.22 μm in diameter. Consequently, the dispersible NGO-PEG could be prepared while the chain length reached a certain extent, and the short chain is unable to stabilize the NGO.
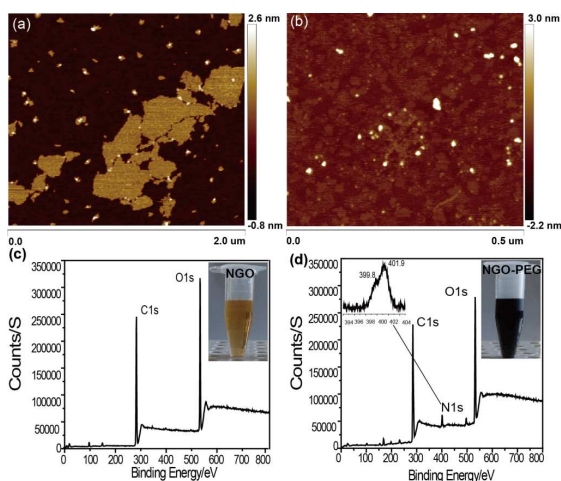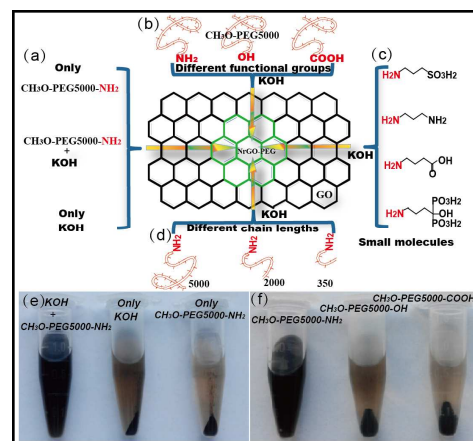
Fig.2 (a-d) Scheme of the synthesis conditions research. (e) Photos of the NGO-PEG samples prepared with only amine-PEG-5000, only KOH, both amine-PEG-5000 and KOH after centrifugation at 7000 r/min for 3 min. (f) Photos of the NGO-PEG samples prepared with different anchor groups after centrifugation at 7000 r/min for 3 min.

Further, the influence of the ratio of GO to KOH and the reaction temperature were investigated for the NGO-PEG synthesis. The solution was subjected to agglomerate under the ratio (m_{GO}: m_{KOH}) at 1:1, 1:2, 1:16, and without noticeable agglomeration at 1:4 and 1:8 after centrifugation at 7000r/min for 3 min (Fig. S2c). Then, the solution reacted at 1:4 and 1:6 slightly intercepted on the membrane, but the reaction at 1:8 did not have a cutoff of 0.22 μm after filtration. The influence of the reaction temperature shows an analogous phenomenon when the temperature increases from 25 °C to 100 °C, NGO-PEG exhibits little agglomeration between 40 °C and 80 °C. However, the solution agglomerated when the temperature was 25 °C or 100 °C. The results showed that too high or too low temperature is not suitable for the PEG attached to the NGO. Nevertheless, the solution reacted at 40 °C and 60 °C slightly intercepted on the membrane, but there is no interception when the temperature increased to 80 °C (Fig. S2d) after filtration. In brief, the optimal reaction conditions are a temperature of 80 °C, the GO to KOH ratio of 1:8 for both PEG-NH2 and KOH present.

Stability is one of the most important parameters that could determine the final destination of nanoparticles when applied in vivo. Nanoparticles without sufficient surface coating tend to aggregate in high salt and protein concentration solution. To demonstrate the stability of NGO and NGO-PEG in physiological conditions, the nanoparticles were dispersed in water, PBS, cell medium (DMEM) or FBS and subsequently centrifuged at 7000 r/min. By way of comparison, it was found that the NGO-PEG exhibited better solubility and stability in a range of physiological solutions including water, PBS, cell medium and FBS. As shown in Fig. 3a, NGO experiences fast aggregation in PBS, cell medium and FBS after centrifugation, which is likely due to screening of the electrostatic charges and nonspecific binding of proteins on the NGO.[45] In short, the attachment of PEG-amine to the NGO plane improves the dispersibility of graphene in physiological conditions to make more potential biological applications.

The covalent binding of BPEI to NGO-PEG was performed using EDC/NHS chemistry. The successful conjugation between the carboxylic group of NGO-PEG and amino group of BPEI were

Fig.1 AFM image of (a) graphene oxide and (b) PEGylation reduced graphene oxide sheets. (c) XPS survey spectra of NGO (inset: photograph of NGO). (d) XPS survey spectra of NGO-PEG, high-resolution N 1s spectrum and photograph of NGO-PEG (inset).

confirmed by ^{1}H NMR analysis and UV/vis spectra analysis (Fig. S3 & Fig. 3b inset). The conjugation efficiency of BPEI was calculated by measuring the UV/vis absorbance calibration curve of cuparammonium complexes formed between BPEI and copper ion (Ⅱ) at 630 nm.[46] The UV standard curve has a good linear relationship, described by the following typical equation: Y=0.0135+0.0012x (R2=0.9948) (Fig. S4). The conjugation ratio of BPEI to NGO-PEG was approximately 0.6:1 by weight based on the added PEI.

Noncovalent interactions including π - π stacking and hydrophobic interactions are widely used to load aromatic chemotherapy drugs on the surface of sp^2-bonded nanocarbons such as graphene and carbon nanotubes. Ce6 as a photosensitizer molecule with a high sensitizing efficacy, has been reported to be loaded onto the surface of graphene successfully via π - π stacking and hydrophobic interactions for PDT of cancer cells.[15] In this study, the Ce6 delivery capacity and PDT efficacy were investigated using NGO-PEG and NGO-PEG-BPEI as carriers. The zeta potentials of NGO-PEG, NGO-PEG-BPEI, NGO-PEG-Ce6 and NGO-PEG-BPEI-Ce6 were determined to be -9.0, 16.0, -13.7 and 3.6 mV (Fig. S5). By the conjugation of positively charged BPEI, the zeta potentials for the NGO-PEG-BPEI and NGO-PEG-BPEI-Ce6 were higher than that for NGO-PEG and NGO-PEG-Ce6 indicates a significant difference in the surface charge. Therefore, the positively charged NGO-PEG-PEI-Ce6 may be more uptake by cancer cells and localize preferentially in the lysosomes and subsequently becoming toxic to cancer cells.[42]

The drug loading capacity of NGO-PEG and NGO-PEG-BPEI were discussed to evaluate the influence of the PEG attached to the graphene plane. Ce6 was mixed with NGO-PEG and NGO-PEG-BPEI in water solution by stirring overnight and the followed purification to remove free Ce6. The UV/vis spectrum of the resultant solution showed an absorption peak at 404 nm, which indicated successful loading of Ce6 onto NGO-PEG and NGO-PEG-BPEI (Fig. 3b). Then, the UV/vis peak at 404 nm was used to determine the concentrations of Ce6 in NGO-PEG-Ce6 and NGO-PEG-BPEI-Ce6 samples after subtraction of absorbance contributed by NGO-PEG and NGO-PEG-BPEI (Fig. 3b inset). Furthermore, the relationship between the feeding concentrations of Ce6 and the amount of Ce6 finally loaded on NGO-PEG and NGO-PEG-BPEI was investigated by UV/vis spectra. It was discovered that the loading capacity (the weight ratio of Ce6: NGO-PEG in the NGO-PEG-BPEI-Ce6 and NGO-PEG-Ce6 sample) of Ce6 on NGO-PEG-BPEI reached a maximum of 26 % compared to 13 % on NGO-PEG at Ce6 concentration about 2 mM (Fig. 3c). These results show that the drug loading capacity of NGO-PEG-BPEI is approximately 2.5 folds higher than that of NGO-PEG on average at a series of feeding concentrations of Ce6, possibly owing to that electrostatic absorption effect was occurred between positively charged NGO-PEG-BPEI and negatively charged Ce6.

The Ce6 loaded on NGO-PEG was notably stable in phosphate buffers with acidic (pH 4.8) and neutral pH (pH 7.4), only approximate 5 % Ce6 release from NGO-PEG in the acidic and neutral solution after 48 h (Fig. 3d). However, the result showed that though the Ce6 loaded on NGO-PEG-BPEI was stable in phosphate buffers with neutral pH, but it release from NGO-PEG-BPEI was accelerated in acidic solutions (pH 4.8), approximate 20 % Ce6 release from NGO-PEG-BPEI in the acidic solution after 48 h (Fig. 3d). Therefore, if the NGO-PEG-BPEI-Ce6 is located in acidic
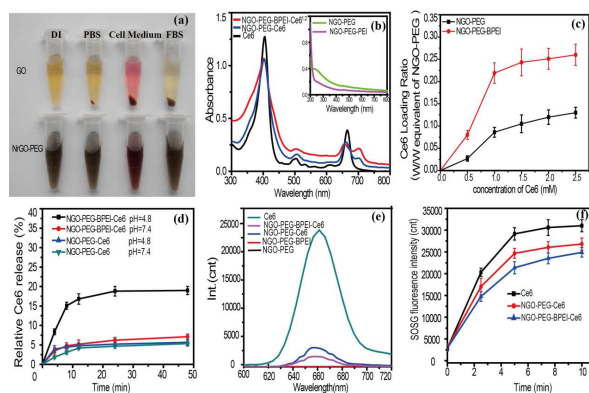
Fig.3 (a) Stability of NGO and NGO-PEG in water, PBS, cell medium and serum, no precipitation was observed after centrifugation at 7000 r/min for 3 min of NGO-PEG. (b) UV/vis spectra of Ce6, NGO-PEG-Ce6 and NGO-PEG-BPEI-Ce6, inset: NGO-PEG and NGO-PEG-BPEI. (c) Relationship between the feeding Ce6 concentrations and the amounts of Ce6 loaded on NGO-PEG and NGO-PEG-BPEI. (d) Release of Ce6 from NGO-PEG-Ce6 and NGO-PEG-BPEI-Ce6 in pH 4.8 and 7.4. (e) Fluorescence spectra of Ce6, NGO-PEG-Ce6, NGO-PEG-BPEI-Ce6, NGO-PEG and NGO-PEG-PEI at 0.2 μM of Ce6 equivalent under 400 nm excitation. (f) Singlet oxygen generation of free Ce6, NGO-PEG-Ce6 and NGO-PEG-BPEI-Ce6 (1 μM) after irradiation with 660 nm laser (0.2 w/cm^2) for different periods of time.

microenvironment, Ce6 should release from NGO-PEG-BPEI to have a superior PDT effect.

The fluorescence spectrum was used to understand the interaction between NGO-PEG/NGO-PEG-BPEI and Ce6. Fig. 3e shows the fluorescence emission spectra of aqueous solution of Ce6, NGO-PEG, NGO-PEG-BPEI, NGO-PEG-Ce6 and NGO-PEG-BPEI-Ce6. It was exposed that 80-90 % of Ce6 fluorescence was drastically quenched once it was loaded onto NGO-PEG or NGO-PEG-BPEI at the same Ce6 concentration, owing to the direct binding of Ce6 onto NGO-PEG/NGO-PEG-BPEI was noncovalent in nature, driven by hydrophobic interactions and π-π stacking[47, 48] between Ce6 and aromatic regions of NGO-PEG/NGO-PEG-BPEI sheet. The quenching degree of NGO-PEG-BPEI-Ce6 is higher than NGO-PEG-Ce6 at equivalent Ce6 concentration, may be due to the interaction between Ce6 and BPEI grafted on the side of NGO-PEG.

Singlet oxygen ($^1O_2$) generation is the critical step in PDT, which can react with singlet oxygen sensor green (SOSG) to generate fluorescence signal. Hence, the generation of singlet oxygen ($^1O_2$) of free Ce6, NGO-PEG-Ce6 or NGO-PEG-BPEI-Ce6 was evaluated under irradiation by measuring the fluorescence signal with 494 nm excitation. The SOSG's fluorescence intensity at 528nm from free Ce6, NGO-PEG-Ce6 and NGO-PEG-BPEI-Ce6 exhibits an exposure time-dependent enhancement, which indicating increased $^1O_2$ generation (Fig. 3f & Fig. S6). Interestingly, although the fluorescence of Ce6 was drastically quenched after it was loaded on NGO-PEG and NGO-PEG-BPEI, the $^1O_2$ production ability of NGO-PEG-BPEI-Ce6 and NGO-PEG-Ce6 remained considerably high. As shown in Fig. 3f, the $^1O_2$ production ability of NGO-PEG-BPEI-Ce6 was approximate ~75-80 % relative to that of free Ce6 and ~80-85 % relative to that of NGO-PEG-Ce6.

HeLa cells were used to test the photodynamic treatment effectiveness of free Ce6, NGO-PEG-Ce6 and NGO-PEG-BPEI-Ce6 in cellular experiments. Cells were incubated with Ce6, NGO-PEG, NGO-PEG-Ce6, NGO-PEG-BPEI and NGO-PEG-BPEI-Ce6 at a series of concentrations for 24 h and subsequently irradiated with a 660 nm laser at a power density of 0.2 W/cm^2 for 5 min. CCK-8 assay was carried out to determine the viabilities of cells at 24 h post various treatments. As expected, there was negligible cell killing effect of NGO-PEG and NGO-PEG-BPEI either in the dark or under light irradiation (Fig. S7a&b). The unirradiated groups of Ce6, NGO-PEG-Ce6 and NGO-PEG-BPEI-Ce6 displayed more over 95 % cell viability, exhibited negligible dark toxicity to HeLa cells at Ce6 concentrations from 0.25 to 2 μM (Fig. S7c), indicating that the free Ce6, NGO-PEG-Ce6 and NGO-PEG-BPEI-Ce6 had no effect on tumor cells without light exposure. In contrast, to the irradiated group, NGO-PEG-Ce6 and NGO-PEG-BPEI-Ce6 exhibited the cancer cell killing effect when irradiated by the 660 nm laser, the PDT effect increased with the Ce6 concentration increasing from 0.25 to 2 μM, indicating a laser irradiation induced concentration-dependent cytotoxicity on tumor cells. Surprisingly, the NGO-PEG-BPEI-Ce6 showed a significantly improved PDT efficacy compared to NGO-PEG-Ce6 and frees Ce6 at all studied concentrations. The data suggest that the NGO-PEG-BPEI-Ce6 nanocarrier have the capability of selective PDT effect on tumor cells (Fig. 4a).

The PDT effects of free Ce6, NGO-PEG-Ce6 and NGO-PEG-BPEI-Ce6 on HeLa cells were also observed using Calcein AM (cytoplasm staining of live cells) and Propidium iodide (nucleus staining of death cells) co-staining. With laser irradiation for 5 min, the control group cells all displayed green fluorescence (Fig. S7d), which suggested that laser irradiation alone can not kill cells. Conversely, the cells treated with NGO-PEG-BPEI-Ce6 were killed and displayed intense homogenous red fluorescence in the nuclei (Fig. 4d). As shown in Fig. 4c, more than half cells treated with NGO-PEG-Ce6

display red fluorescence, which indicated most cells were killed. Meanwhile, few cells were dead in free Ce6 group (Fig. 4b) at equivalent Ce6 concentration (2 μM). The above results are consistent with CCK-8 assay.

In order to understand why the PDT effect using NGO-PEG-BPEI-Ce6 was much better than that of NGO-PEG-Ce6 and free Ce6, we performed flow cytometric analysis, confocal microscopy and fluorescence microscope experiments to study the cellular uptake behavior, intracellular localization and ROS producing ability. HeLa cells were used to investigate the cellular uptake behavior under flow cytometry. The intracellular fluorescence show time-dependent increased for free Ce6, NGO-PEG-Ce6 and NGO-PEG-BPEI-Ce6 incubated cells (Fig. 5a-c). However, the fluorescence intensity of Ce6 in NGO-PEG-BPEI-Ce6 group is always significantly higher than that in the NGO-PEG-Ce6 and free Ce6 group at all the examined time points although the fluorescence quenching of Ce6 attached on NGO-PEG-BPEI. The mean fluorescence intensity (6.66 $\times 10^5$ au) of Ce6 in NGO-PEG-BPEI-Ce6 system was 2.6-fold stronger than that in NGO-PEG-Ce6 (2.54×10^5 au), and 30-fold stronger than that in free Ce6 system (2.23×10^4 au) after 24 h incubation (Fig. 5d). We speculate that the significantly enhanced Ce6 delivery by NGO-PEG-BPEI-Ce6 and NGO-PEG-Ce6 may be the internalization efficiency of them through endocytosis than passive diffusion of Ce6 into cells.

To verify the uptake mechanism of NGO-PEG-BPEI-Ce6 and NGO-PEG-Ce6, the HeLa cells were incubated with NGO-PEG-BPEI-Ce6 and NGO-PEG-Ce6 at low temperature (4 ⬚), which would inhibit the cellular endocytosis.[49, 50] The fluorescent images showed that the uptake of NGO-PEG-BPEI-Ce6 and NGO-PEG-Ce6 were significantly depressed at 4 ⬚ compared to that at 37 ⬚ after 2 h
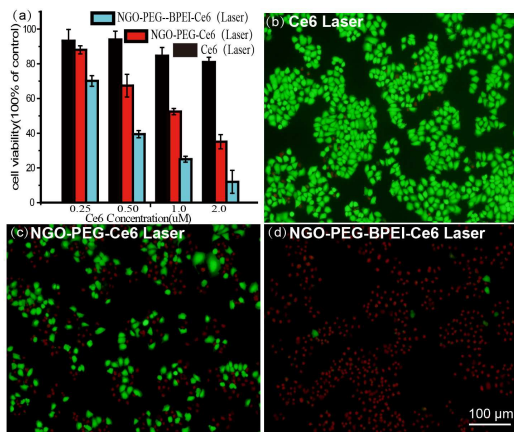
Fig.4 (a) Relative cell viability data obtained from the CCK-8 assay of HeLa cells after treatment with Ce6, NGO-PEG-Ce6 and NGO-PEG-BPEI-Ce6 with light irradiation by 662 nm laser at a power density of 0.2 W/cm^2 for 5 min, the cell viability values were all normalized to control untreated cells. (b-d) Fluorescence image of calcein/propidium iodide stained HeLa cells incubated with 2 μM free Ce6, NGO-PEG-Ce6 and NGO-PEG-BPEI-Ce6 for 24 h after laser irradiation. Error bars were based on SD of triplicate parallel samples.
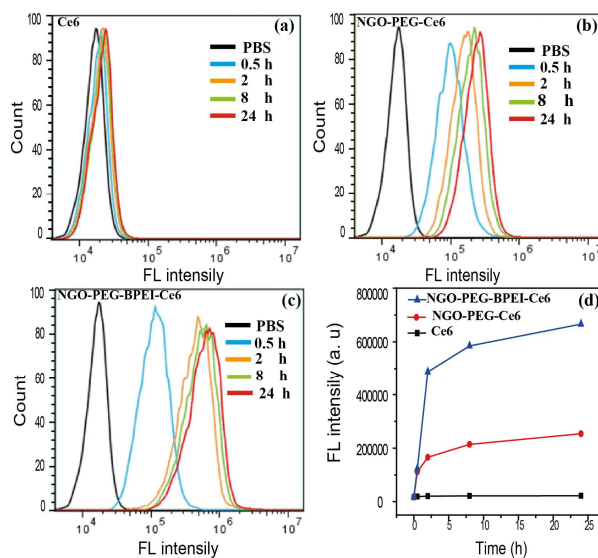
Fig.5. Flow cytometric analysis of mean fluorescence intensity (1×10^4 cells) in HeLa cells incubated with (a) Ce6, (b) NGO-PEG-Ce6 and (c) NGO-PEG-BPEI-Ce6 at equivalent Ce6 concentration 2 μM for 0.5,2,8,24 h. (d) The changes of Ce6 fluorescence intensity in cells as a function of incubation time.

(Figure. S8), suggesting NGO-PEG-BPEI-Ce6 and NGO-PEG-Ce6 may be internalized via energy-dependent endocytosis.

To investigate the intracellular localization of free Ce6, NGO-PEG-Ce6 and NGO-PEG-BPEI-Ce6 after endocytosis by cells, experiments were performed with HeLa cells treated with free Ce6, NGO-PEG-Ce6 and NGO-PEG-BPEI-Ce6 at equivalent Ce6 concentration (2 μM) for 24 h. Hoechst is a blue fluorescent dye that stains the cell nucleus, Lysotracker is a green fluorescent dye that stains the acidic lysosomes. Mitotracker is a green fluorescent dye that stains the mitochondria. Hence, the potential colocalization between Ce6 (red) and lysosomes (green)/ mitochondria (green) should yield a yellow/orange overlap when the images are merged. The CLSM results showed that there wasn't yellow/orange overlap observed between Lysotracker (Fig. 6 first & second line) or Mitotracker (Fig. S9 first & second line) in cells treated with free Ce6 and NGO-PEG-Ce6, which suggested that Ce6 and NGO-PEG-Ce6 may be dispersed in the cytoplasm. Interestingly, NGO-PEG-PEI-Ce6 was localized in lysosome as observed a yellow/orange overlap yield (Fig. 6 last line), which indicated that NGO-PEG-BPEI could target delivery the Ce6 into lysosome.

The produced ROS level of free Ce6, NGO-PEG-Ce6 and NGO-PEG-BPEI-Ce6 were measured by DCFH-DA method with fluorescence microscope. As expected, negligible fluorescence signal was observed for the cells treated with free Ce6, NGO-PEG-Ce6 and NGO-PEG-BPEI-Ce6 without irradiation (Fig. S10b-d). For the irradiation groups, as shown in Fig. 7, there was little fluorescence signal for the control group (PBS) with laser irradiation (Fig. 7a) or without irradiation (Fig. S10a). However, at the equivalent Ce6 concentration (1μM), NGO-PEG-BPEI-Ce6 (Fig. 7e) had a higher fluorescence signal of than NGO-PEG-Ce6 (Fig. 7b) and free Ce6 (Fig. 7d) with laser irradiation, which exhibited the best ROS producing ability. Interestingly, we observed that large vesicles were produced from the cells treated with NGO-PEG-BPEI-Ce6, as shown in Fig. 7f & Fig. S11, but little vesicle was observed in those treated with NGO-PEG-Ce6 (Fig. 7c) , and no vesicle was observed in those treated with free Ce6 (Fig. S10e). We hypothesized that the
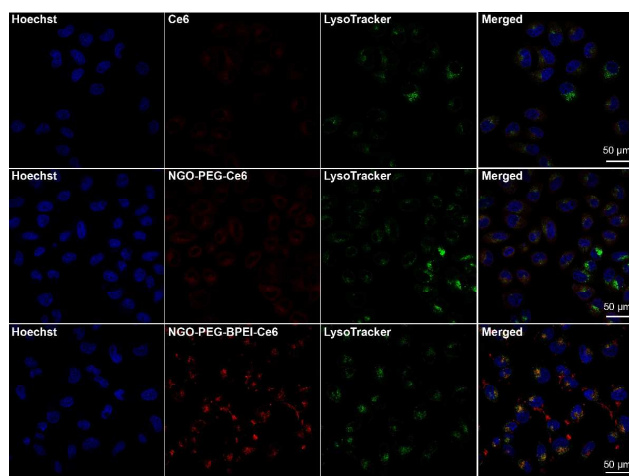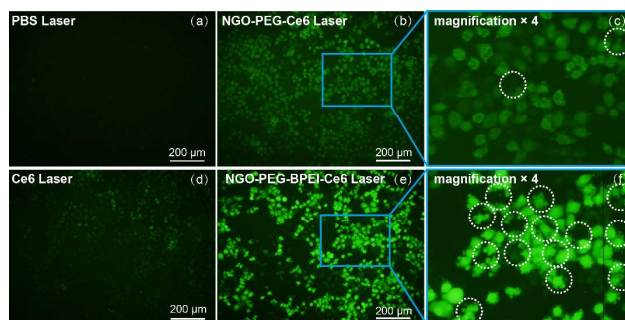
Fig.7 Fluorescence image of determination ROS producing ability by DCFH-DA method with fluorescence microscope incubated with PBS (a), 1 μM free Ce6 (d), equivalent amount of NGO-PEG-Ce6 (b, c) and NGO-PEG-BPEI-Ce6(e, f) for 24 h after laser irradiation.

vesicles might be induced by the following two mechanisms. In one mechanism, NGO-PEG-BPEI-Ce6 localize in the structures of lysosomes, under irradiation, Ce6 localizing in lysosomes breakdown their membrane or inactivate the matrix proteases, and the release of proteolytic enzymes triggers mitochondrial apoptosis Bid cleavage, [51] so these vesicles may be the apoptosis globules that form in mitochondrial apoptosis progress.[32] For another mechanism, Ce6 localized in lysosome can induce autophagy and the consequent autophagosomes formation. Actually, the completion of the autophagic process requires autophagolysosomes formation following the autophagosome-lysosome fusion.[32-33] Therefore, the vesicles may be fusion vesicles of autophagosome-lysosome. The above result indicates that the lysosomes target properties of NGO-PEG-BPEI-Ce6 was notably useful to improve the therapeutic efficacy of PDT. In addition, the exact mechanism of the vesicles formation still remains unclear and requires further study in the future.

Based on the results of cellular uptake behavior, intracellular localization and ROS producing ability, we hypothesise that there are two main reasons for the remarkably improved PDT efficiency of NGO-PEG-BPEI-Ce6 compared to NGO-PEG-Ce6 and free Ce6. Firstly, NGO-PEG-BPEI-Ce6 delivered more Ce6 into the cells than that of free Ce6 and NGO-PEG-Ce6 at the same Ce6 concentration. We confirm that the significantly enhanced Ce6 delivery due to the efficient cell entry of NGO-PEG-BPEI and NGO-PEG through endocytosis that shuttles Ce6 into cells, while free Ce6 has less effective intracellular cross-membrane diffusion ability. Next, NGO-PEG-Ce6 and free Ce6 can only act photodynamic efficacy in cytoplasm. Whereas the NGO-PEG-BPEI-Ce6 could be engulfed into cytoplasm and then gradually turned into lysosomes, then, Ce6 was released from NGO-PEG-BPEI-Ce6 because of the acidic microenvironment in lysosomes (PH 4~5), and a few released Ce6 escaped from lysosomes into cytoplasm. Subsequently, the photodynamic efficacy was achieved in both lysosomes and cytoplasm under light irradiation and improve the efficacy of PDT.[52]

Conclusions

In conclusion, we found that NGO can experience quick PEGylation in alkali solutions at moderate temperatures. This interesting reaction provides a green route to synthesize NGO-PEG with excellent dispersibility in water and physiological conditions. Considering that the nontoxic KOH is readily available, this study

Fig.6 Localization image of Ce6, NGO-PEG-Ce6 and NGO-PEG-BPEI-Ce6 stained HeLa cells, incubated with free Ce6, NGO-PEG-Ce6 and NGO-PEG-BPEI-Ce6 (Ce6, 2 μM) after 24 h (Lysotracker stained lysosomes).

opens an exciting opportunity to produce NGO-PEG on an industrial scale. The results from AFM, XPS, UV/vis and fluorescence spectrum clearly indicate that the PEG-amine was coupled to the surface of the graphene successfully. Moreover, NGO-PEG-BPEI was easily synthesized via EDC/NHS chemistry. Compared with NGO-PEG, the NGO-PEG-BPEI shows the following features: firstly, the NGO-PEG-BPEI shows higher loading capability (about 2.5-fold) for photosensitizer Ce6 via π-π stacking. Additionally, the NGO-PEG-BPEI-Ce6 dramatically improved photodynamic efficacy due to the increased cellular uptake, targeting accumulation of Ce6 in lysosomes and consequent higher ROS producing ability. The results indicated the potential applications of NGO-PEG-BPEI in targeting PDT and facilitate the manipulation and processing of graphene-based materials for different applications. To further improve the performance of the NGO-PEG-BPEI nanocarrier in drug delivery therapy, specific biomarkers and systemically assess the toxicity shall be undertaken to.

Materials and methods

Materials

Graphite powder was purchased from Acros. $KMnO_4$ (AR), $NaNO_3$ (AR), H_2O_2 (technical grade, 30 %), linear chain PEG amine (MW350, 2000, 5000), branched polyethylenimine (BPEI), N-(3-Dimethylaminopropyl)-N-ethylcarbodiimide (EDC), N-Hydroxysuccinimide (NHS), were purchased from Sigma-Aldrich. Chlorin e6 (Ce6) was purchased from Frontier Scientific Inc. Dulbecco's modified Eagle's medium (DMEM), fetal bovine serum (FBS), penicillin-streptomycin, trypsin were obtained from Gibco. Calcein AM, Propidium iodide and CCK-8 kit were purchased from Dojindo. ROS kit (DCFH-DA), singlet oxygen sensor green (SOSG), Mitotracker, Lysotracker, Hoechst were purchased from Molecular Probes. All other chemical reagents were used without any further purification. Deionized water (Millipore Milli-Q grade) with a resistivity of 18.2 MU cm was used in all the preparations.

Synthesis of GO, NGO-PEG and NGO-PEG-BPEI

Preparation of GO: Graphene was synthesized using the modified Hummers method.[43] Concentrated H_2SO_4 (70 mL) was added to graphite (0.4 g) , and the mixture was cooled using an ice bath to 0 ° C, $KMnO_4$ (4 g) and $NaNO_3$ (0.6 g) were added separately to the mixture with stirring, continue a period of 10 minutes, the reaction was warmed to 35 ° C and stirred for 30 min. Next, 50 mL distilled water were added slowly drop by drop. Producing a large exotherm to 95 ° C and stirred for 30 min, afterwards, the reaction was ended by a final addition of 100ml distilled water and 8 mL 30 % H_2O_2 solution. For purification, the resulting mixture was washed multiple times, first with 10 % HCl solution four times and subsequently with DI water two times. The resulting suspension was centrifugated and filtered over a PTFE membrane with a 0.45 μ m pore size. The obtained solid on the filter was vacuum-dried overnight at 70 ° C. X-ray diffraction (XRD) analysis was employed to verify the produce of GO. To obtain NGO, the above solid GO was cracked by ultrasonic probe at 500 W for 2 h. AFM was acquired to check the morphology of the produced NGO.

Preparation of NGO-PEG : NGO-PEG was synthesized by an epoxide ring-opening reaction between GO and line chain amine-terminated PEG (average molecularweight: 5000). Firstly, 10 mL GO suspension (0.5 mg/mL) was subjected to ultrasonication for 2 h;

then, PEG-amine （30 mg） and KOH （40 mg） were added into the homogeneous and transparent GO dispersion in water. Finally, the homogeneous solution was vigorously stirred at 80 ° C for 24 h. The resulting NGO-PEG was subsequently centrifuged, dialyzed in water with molecular weight cut off of 10 kDa filter (Millipore Inc) for 24 h. Condition experiments was keep under the same conditions as the above experimental group except for adjusting relevant conditions such as reagents, ratios, temperature and so on.

Preparation of NGO-PEG-BPEI: Branched polyethylenimine (BPEI) was covalently to NGO-PEG by using cross-linking reagents EDC and NHS. Firstly, 60 mg EDC and 30 mg NHS were mixed in 10 mL NGO-PEG (2 mg/mL, from mass of freeze drier) solution and magnetically stirred at room temperature for 15 min. After activation, 20 mg BPEI (MW 1800 from Sigma-Aldrich) was added in the solution to react at room temperature for 24 h. Finally, the unreacted BPEI was removed by filtration through a 10 kDa filter (Millipore Inc) and repeatedly washed with phosphate buffer (PBS, pH=7.4). Then, in order to remove the conjugated BPEI which was possibly adsorbed on the plane of graphene, NGO-PEG-BPEI was washed with 50% isopropanol several times until no PEI could be detected in the filtrate by measuring the cuprammonium complex formed between PEI and copper ion(II) at 630 nm using UV/Vis spectrophotometry,[46] then dispersed in H_2O to obatin desired concentration.

Synthesis of NGO-PEG-Ce6 and NGO-PEG-BPEI-Ce6

For preparation of NGO-PEG-Ce6, Ce6 was dissolved in DMSO at 10 mM as the stock solution for further use. 500 μL NGO-PEG (1.0 mg/mL) and 200 μL Ce6 (10 mM) were mixed in a 2 mL PBS solution and magnetically stirred at room temperature for 12 h. The excess Ce6 was removed by dialysing in PBS solution through a 10 kDa dialysis membrane for 24 h until the filtrate became free of green color. For preparation of NGO-PEG-BPEI-Ce6, The procedures were the same as that for NGO-PEG-Ce6 except using NGO-PEG-BPEI (equal amount NGO-PEG, 1.0 mg/mL) dispersed in PBS solution.

Materials characterization

Atomic force micrographs (AFM) were obtained using a Multimode Nano in the tapping mode. XRD patterns were acquired from dried nanoparticle samples with a Persee XD3 X-raydiffractometer using Cu NF radiation at 36 kV and 20 mA. X-Ray photoelectron spectroscopy (XPS) measurement was performed using a multipurpose surface analysis system (Scientific Escalab 250, Thermo, UK). The photoelectron spectra were excited by an Al Ka (1486.6 eV) anode operating at 100 W. The base pressure during XPS analysis was maintained at less than 10-9 mbar. Ultraviolet-visible (UV/vis) spectra were recorded with UV-3600 spectrophotometer with a 10-mm quartz cell, where the light path length was 1 cm. The absorbance at 404 nm was used as the characterization peak to confirm successful conjugation of Ce6. The concentration of Ce6 loaded on GO-PEG and GO-PEG-PEI was determined by UV/vis spectra at 404 nm with a molar extinction coefficient of 1.1×10^5 $M^{-1}cm^{-1}$ after subtracting the absorbance contributed by GO-PEG and GO-PEG-PEI at the same wavelength.[15] Fluorescence spectra of free Ce6, GO-PEG-Ce6 and GO-PEG-PEI-Ce6 were measured using near-infrared fluorescence spectrograph (Thermo Fisher) under 400 nm excitation, and the SOSG fluorescence spectra were measured under 494 nm excitation.

Singlet oxygen detection

The generation of singlet oxygen was determined with singlet oxygen sensor green (SOSG). Free Ce6, NGO-PEG-Ce6 or NGO-PEG-PEI-Ce6 was fixed at Ce6 concentration 1.0 μM equivalent concentrations. SOSG was dissolved in water containing 2 % methanol with the final concentration of 1.0 μM, and subsequently irradiated by 660 nm laser at the light power density of 0.2 W/cm^2 for different periods of time. SOSG fluorescence was produced using an excitation wavelength of 494 nm with a fluorescence spectrum. The singlet oxygen level of the sample was evaluated by the SOSG fluorescence enhancement compared with the background or control samples.

Photodynamic treatment and cell toxicity assay

The HeLa cells were cultured in a humidified atmosphere (5 % CO$_2$) at 37 ℃, and grown in DMEM medium supplemented with 10 % FBS. For cell viability assay, HeLa cells were pre-cultured in 96-well cell culture plates at 5000 for 24 h; and then added with free Ce6, NGO-PEG-Ce6 or NGO-PEG-PEI-Ce6 at a series of concentrations. After incubation for 24 h, the cells were washed with PBS to remove the residual materials; and subsequently cells were irradiated by the 660 nm laser at a power density of 0.2 W/cm^2 for 5 min. After another 24 h of incubation, the standard CCK-8 assay was performed on multiskan spectrum (Thermo Fisher) to determine the cell viabilities relative to the control untreated cells (incubated with the same volume of PBS).

The PDT effects of free Ce6, NGO-PEG-Ce6 or NGO-PEG-PEI-Ce6 on HeLa cells were further verified using Calcein AM and Propidium iodide (PI). Cells (1×10^5 cells per well) were seeded in 6-well plates and incubated overnight. Then, incubated with PBS, free Ce6, NGO-PEG-Ce6 or NGO-PEG-PEI-Ce6 (Ce6 concentration=2 μM) for 24 h, cells were then irradiated with a 660 nm laser at a power density of 0.2 W/cm^2 for 5 min, after incubation for 24 h, Calcein AM/propidium iodide was added. Fluorescence image of Calcein AM/propidium iodide staining were observed under fluorescence microscope (DMLRB inverted microscope, Leica).

Cell uptake assay and intracellular localization

HeLa cells were cultured in 35 mm culture dishes containing NGO-PEG-PEI-Ce6, NGO-PEG-Ce6 or free Ce6 at the same Ce6 concentration (2 μM) for different incubation time points (0.5, 2, 8 and 24 h) at 37 ℃. Then, cells were washed with PBS three times, trypsinized, and resuspended with medium, harvested using a centrifuge, and at last dispersed in 500 μL PBS. Flow cytometry analysis (Epics XL-MCL, Beckman coulter) was used to analyse the fluorescence intensity of cells incubated with Ce6, NGO-PEG-Ce6 and NGO-PEG-PEI-Ce6 under 400 nm excitation. The cellular uptake mechanism experiment of NGO-PEG-Ce6 and NGO-PEG-PEI-Ce6 were performed at 4°C, cells incubated with NGO-PEG-Ce6 and NGO-PEG-PEI-Ce6 (2 μM) for 2h before imaged under a confocal fluorescence microscope.

HeLa cells (1×10^5 cells) were cultured with NGO-PEG-PEI-Ce6, NGO-PEG-Ce6 or free Ce6 (Ce6 concentration=2 μM) in culture dishes. After washing the cells three times with PBS (pH 7.4), the cells were stained by Hoechest and Lysotracker/ Mitotracker and observed by a laser scanning confocal microscope (FLUOVIEWFV10i Olympus) with 404 nm laser excitation. The emission was collected from 580 to 720 nm.

ROS detection

Intracellular ROS generation was measured by DCFH-DA method. The HeLa cells were cultured in 24 well plates (5×10^4 cells/ml) with media containing Ce6 concentrations 1.0 μM of free Ce6, NGO-PEG-Ce6 or NGO-PEG-PEI-Ce6 for 24 h,   followed by exposed to 660 nm Laser (0.2 W/cm^2) for 5 min, and then the cells were washed with PBS three times and incubated with 10 μM DCFH-DA at 37 ℃ for 30 min. The DCFH-DA is diffused into cells and is deacetylated by cellular esterases to non-fluorescent DCFH, which is rapidly oxidized to highly fluorescent DCF by ROS. To measure the intracellular reactive oxygen species (ROS), the DCF fluorescence was excited by excitation at 488 nm and emission 525 nm observed under fluorescence microscope (DMLRB inverted microscope, Leica).

Acknowledgements

Notes and references

1 K. S. Novoselov, A. K. Geim, S. V. Morozov, D. Jiang, Y. Zhang, S. V. Dubonos, I. V. Grigorieva and A. A. Firsov, *Science.*, 2004, **306**, 666-669.
2 N. Xiao, X. Dong, L. Song, D. Liu, Y. Tay, S. Wu, L. J. Li, Y. Zhao, T. Yu, H. Zhang, W. Huang, H. H. Hng, P. M. Ajayan and Q. Yan, *ACS Nano.*, 2011, **5**, 2749-2755.
3 H. Wang, J. T. Robinson, G. Diankov, H. Da, *J. Am. Chem. Soc.*, 2010, **132**, 3270-3271.
4 X. Huang, Z. Yin, S. Wu, X. Qi, Q. He, Q. Zhang, Q. Yan, F. Boey and H. Zhang, *Small.*, 2011, **7**, 1876-1902.
5 D. Li and R. B. Kaner, *Science.*, 2008, **320**, 1170-1171.
6 G. Eda, G. Fanchini and M. Chhowalla, *Nat. Nanotechnol.*, 2008, **3**, 270-274.
7 F. M. Koehler, N. A. Luechinger, D. Ziegler, E. K. Athanassiou, R. N. Grass, A. Rossi, C. Hierold, A. Stemmer and W. J. Stark, *Angew. Chem. Int. Ed.*, 2009, **48**, 224-227.
8 X. Li, X. Wang, L. Zhang, S. Lee and H. Dai, *Science.*, 2008, **319**, 1229-1232.
9 S. Stankovich, D. A. Dikin, G. H. Dommett, K. M. Kohlhaas, E. J. Zimney, E. A. Stach, R. D. Piner, S. T. Nguyen and R. S. Ruoff, *Nature.*, 2006, **442**, 282-286.
10 W. Zhang, Z. Y. Guo, D. P. Huang, Z. M. Liu, X. Guo and H. Q. Zhong, *Biomaterials.*, 2011, **32**,8555-8561.
11 C. H. Lu, H. H. Yang, C. L. Zhu, X. Chen and G. N. Chen, *Angew.Chem. Int. Ed.,* 2009, **48**, 4785-4787.
12 N. Mohanty and V. Berry, *Nano.Lett.,* 2008, **8**, 4469-4476.
13 Z. Liu, J. T. Robinson, X. Sun and H. Dai, *J. Am. Chem. Soc.,* 2008, **130**, 10876-10877.
14 L. M. Hollanda, A. O. Lobo, M. Lancellotti, E. Berni, E. J. Corat and H. Zanin, *Mat. Sci. Eng. C-Mate.,* 2014, **39**, 288-298.
15 B. Tian, C. Wang, S. Zhang, L. Feng and Z. Liu, *ACS Nano.,* 2011, **5**, 7000-7009.
16 M. P. Monopoli, C. Aberg, A. Salvati and K. A. Dawson, *Nat. Nanotechnol.*, 2012, **7**, 779-786.

17 S. Naahidi, M. Jafari, F. Edalat, K. Raymond, A. Khademhosseini, P. Chen, *J. Control. Release.,* 2013, **166**, 182-194.

18 X. Qi, K. Y. Pu, H. Li, X. Zhou, S. Wu, Q. L. Fan, B. Liu, F. Boey, W. Huang and H. Zhang, *Angew. Chem. Int. Ed*., 2010, **49**, 9426-9429.

19 Y. Si and E. T. Samulski, *Nano. Lett*., 2008, **8**, 1679-1682.

20 X. Yang, Y. Tu, L. Li, S. Shang and X. M. Tao, *ACS. Appl. Mater. Inter.,* 2010, **2**, 1707-1713.

21 J. Liu, L. Tao, W. Yang, D. Li, C. Boyer, R. Wuhrer, F. Braet and T. P.Davis, *Langmuir*., 2010, **26**,10068-10075.

22 S. Park, N. Mohanty, J. W. Suk, A. Nagaraja, J. An, R. D. Piner, W. Cai, D. R. Dreyer, V. Berry and R. S. Ruoff, *Adv. Mater.,* 2010, **22**, 1736-1740.

23 H. Hu, J. Yu, Y.Li, J. Zhao and H. Dong, *J. Biomed. Mater. Res.,* 2012, **100**, 141-148.

24 H. Peng, L. B. Alemany, J. L. Margrave and V. N. Khabashesku, *J. Am. Chem. Soc.,* 2003, **125**, 15174-15182.

25 K. Yang, L. Feng, H. Hong, W. Cai and Z. Liu, *Nat. Protoc.,*2013, **8**, 2392-2403.

26 X. B. Fan, W. C. Peng, Y. Li, X. Li, S. L. Wang, G. L. Zhang and F. B. Zhang, *Adv. Mater.,* 2008, **20**, 4490-4493.

27 Z. Huang, H. Xu, A. D. Meyers, A. I. Musani, L. Wang, R. Tagg, A. B. Barqawi and Y. K. Chen, *Technol. Cancer. Res. T.,* 2008, **7**, 309-320.

28 P. Vijayaraghavan, C. H. Liu, R. Vankayala, C. S. Chiang and K. C. Hwang, *Adv. Mater.,* 2014, **26**, 6689-6695.

29 D. E. Dolmans, D. Fukumura and R. K. Jain, *Nat. Rev. Cancer.,* 2003, **3**, 380-387.

30 B. W. Henderson and T. J. Dougherty, *Photochem and Photobiol.,* 1992, **55**, 145-157.

31 J. Ge, M. Lan, B. Zhou, W. Liu, L. Guo, H. Wang, Q. Jia, G. Niu, X. Huang, H. Zhou, X. Meng, P. Wang, C. S. Lee, W. Zhang, X. Han, *Nat. Commun.,* 2014, **5**, 4596.

32 V. Inguscio, E. Panzarini and L. Dini, Cells., 2012, **1**, 464-491.

33 D. H. Kessel, M. Price, J. J. Reiners. Jr, *Autophagy.,* 2012, **8**, 1333-1341.

34 X. Liang, X. Li, X. Yue and Z. Dai, *Angew. Chem. Int. Ed.,* 2011, **123**, 11826-11831.

35 D. K. Chatterjee, L. S. Fong and Y. Zhang, *Adv. Drug. Deliver. Rev.,* 2008, **60**, 1627-1637.

36 P. Huang, J. Liu, S. J. Wang, Z. J. Zhou, Z. M. Li, Z. Wang, C.L. Zhang, X. Y. Yue, G. Niu, M. Yang, D. X. Cui and X. Y. Chen, *Biomaterials*., 2013, **34**, 4643-4654.

37 P. Rong, K. Yang, A. Srivastan, D. O. Kiesewetter, X. Yue, F. Wang, L. Nie, A. Bhirde, Z. Wang, Z. Liu, G. Niu, W. Wang and X. Chen, *Theranostics*., 2014, **4**, 229-239.

38 A. Sahu, W. I. Choi, J. H. Lee and G. Tae, *Biomaterials.,* 2013, **34**, 6239-6248.

39 D. A. Dikin, S. Stankovich, E. J. Zimney, R. D. Piner, G. H. Dommett, G. Evmenenko, S. T. Nguyen, R. S. Ruoff, Nature., 2007, **448**, 457-460.

40 H. Kim and W. J. Kim, *Small*., 2014, **10**, 117-126.

41 L. Zhang, J. Xia, Q. Zhao, L.Liu and Z. Zhang, *Small*., 2010, **6**, 537-544.

42 A. Asati, S. Santra, C. Kaittanis and J. M. Perez, *ACS Nano.,* 2010, **4**, 5321-5331.

43 D. C. Marcano, D. V. Kosynkin, J. M. Berlin, A. Sinitskii, Z. Sun, A. Slesarev, L. B. Alemany, W. Lu and J. M. Tour, *ACS Nano*., 2010, **4**, 4806-4814.

44 H. Yang, C. Shan, F. Li, D. Han, Q. Zhang and L. Niu, *Chem. Commun.,* 2009, 3880-3882.

45 N. W. Kam and H. Dai, *J. Am. Chem. Soc.,* 2005, **127**, 6021-6026.

46 F. Ungaro, G. De Rosa, A. Miro and F. Quaglia, *J. Pharmaceut. Biomed.,* 2003, **31**, 143-149.

47 R. J. Chen, Y. Zhang, D. Wang and H. Dai, *J. Am. Chem. Soc*., 2001, **123**, 3838-3839.

48 Z. Liu, X. Sun, N. Nakayama-Ratchford and H. Dai, *ACS Nano.,* 2007, **1**, 50-56.

49 L. Y. Chou, K. Ming and W. C. Chan,. *Chem. Soc. Rev.,* 2011, **40**, 233-245.

50 F. Wang, Y. C. Wang, S. Dou, M. H. Xiong, T. M. Sun and J. Wang , *ACS Nano.,* 2011, **5**, 3679-3692.

51 J. J. Jr. Reiners, J. A. Caruso, P. Mathieu, B. Chelladurai, X. M. Yin, D. Kessel, Cell Death Differ., 2002, **9**, 934-944.

52 D. Kessel, J. Natl. Compr. Canc. Ne., 2012, **10**, 56-59.

Graphical Abstract

A fast, facile and mass production method was reported to obtain stable and disperse polyethylene glycol (PEG) modified nanographene (NGO-PEG). Branched polyethylenimine (BPEI) was used to modify the NGO-PEG (NGO-PEG-BPEI) for further application. The NGO-PEG-BPEI-Ce6 exhibited enhanced PDT efficacy compared with NGO-PEG-Ce6 and free Ce6.